Nonlinear Dyn
https://doi.org/10.1007/s11071-021-07102-x

ORIGINAL PAPER

Cross-section deformation, geometric stiffening, and locking in the nonlinear vibration analysis of beams

Ahmed E. Eldeeb · Dayu Zhang · Ahmed A. Shabana

Received: 6 August 2021 / Accepted: 20 November 2021

Abstract Stiff behavior of more general finite element (FE) beam formulations in some problems can be misinterpreted as *locking* based on comparison with simplified analytical and/or less general FE beam formulations. This paper demonstrates that, in more general beam formulations, higher stiffness can be attributed to *geometric nonlinearities* as result of cross-section deformations, not properly captured by analytical or less general FE beam formulations. Limitations of the *ad hoc approaches* used in conventional FE beam formulations to account for beam cross-section deformations are identified, their inconsistency with theory of continuum mechanics is explained, and their appropriateness is evaluated in view of a more general approach. Effect of using different constitutive models on the stiff behavior of beams is investigated, and it is demonstrated that the stiff behavior resulting from the *geometric stiffening* due to the coupling between the *cross-section deformations* and beam vibrations in more general beam formulations cannot always be interpreted as locking. Relationship between geometric stiffening, cross-section deformation, locking, and constitutive model in more general FE beam formulation is explained. Several numerical examples are used to perform static, dynamic, and thermal analyses; and the results obtained are compared with FE commercial software. These results demonstrate limitations of beam formulations used in commercial FE software, shed light on problems of using simplified analytical solutions for verification, highlight concerns of using conventional FE approaches for soft robots and materials, and caution against misinterpretation of the stiff behavior as locking when using more general beam formulations.

Keywords Cross-section deformation · Geometric stiffening · Locking · Coupled deformation modes · Absolute nodal coordinate formulation

A. E. Eldeeb · A. A. Shabana (✉)
Department of Mechanical and Industrial Engineering, University of Illinois at Chicago, 842 West Taylor Street, Chicago, IL 60607, USA
e-mail: shabana@uic.edu

A. E. Eldeeb
e-mail: aeldee2@uic.edu

A. E. Eldeeb
Department of Mechanical Design and Production, Faculty of Engineering, Cairo University, Giza, Egypt

D. Zhang
School of Astronautics, Northwestern Polytechnical University, Xi'an 710072, Shaanxi, People's Republic of China
e-mail: dyzhang@mail.nwpu.edu.cn

1 Introduction

Beam vibration solutions obtained using more general finite element (FE) formulations may exhibit a stiff

Published online: 20 January 2022

behavior that can be misinterpreted as *locking*. Such a misinterpretation in some problems such as axial-deformation problems can be made when more general solutions are compared to solutions obtained using analytical methods that employ simplifying assumptions or with solutions obtained using less general FE formulations. For example, rigid cross-section assumption is made in classical beam formulations, as in case of Euler–Bernoulli beam theory, which neglects shear deformation and assumes rigid cross section remains normal to beam neutral axis. In Timoshenko beam theory, on the other hand, rigid cross section is allowed to rotate as result of the shear. Therefore, in classical beam vibration problems, analytical solutions based on simplified approaches do not consider beam cross-section deformation [1–10].

In more general FE beam formulations such as *absolute nodal coordinate formulation* (ANCF), there is a relation between geometric stiffening, cross-section deformation, locking, and constitutive model. Geometric stiffening can be due to kinematic coupling between different modes of displacements. Coupling between cross-section deformation and axial and bending deformations is one example. Another example is axial/bending deformation coupling which was considered in field of rotor dynamics. These coupled deformation modes can cause numerical and convergence problems in case of stiff and thin structures using plane strain constitutive models [11]. However, linearization and ignoring these coupled deformation modes lead to wrong results in case of large deformation and soft materials. Locking is a phenomenon that can be addressed using different approaches. Detailed discussion on locking and locking alleviation techniques in conventional and ANCF elements can be found in [12]. However, it was demonstrated that modifying constitutive model for three-dimensional ANCF beam element based on continuum mechanics approach can improve its performance [13]. In this case, three-dimensional ANCF beam element does not suffer from shear locking using this modification.

In a realistic motion scenario, beam stretch or bending leads to a change in cross-section dimensions. Such a change, resulting from the coupling between cross-section deformations and the stretch and bending, produces *geometric stiffening* that has direct influence on the vibration amplitude, a phenomenon that has been recognized for decades, particularly in the area of rotor dynamics [14]. Ignoring such coupled deformation modes does not only lead to inaccurate results in case of large deformation and very flexible structures [11] but can also in addition to ignoring axial/bending deformation coupling, as shown in Fig. 1, falsely lead to unstable solutions which are not supported by experimental observations of actual motion scenarios [15–24]. The results presented in Fig. 1 also shed light on problems associated with using linearization techniques in stability analysis of highly nonlinear mechanical and aerospace systems. The eigenvalue analysis based on linearized equations can lead to misleading stability information. In some studies, reported in the literature, the focus has been on geometric stiffening that results from the coupling between axial and bending deformations. It was demonstrated that linearization of rotor blade equations that leads to ignoring axial/bending coupling produces wrong unstable solution.

In order to clearly define scope of this investigation, a simple cantilever beam subjected to an axial force at its free end is considered. Figure 2 shows a comparison between predicted axial deformation using nonlinear ANCF finite elements and FE commercial software ANSYS. Results of this figure show that *plane strain* assumption under-predicts a solution that does not agree well with ANSYS solution, while the *plane stress* assumption leads to a solution in a good agreement with ANSYS solution. This stiff behavior of ANCF plane-strain solution can be misinterpreted as locking due to poor element performance. The stiff

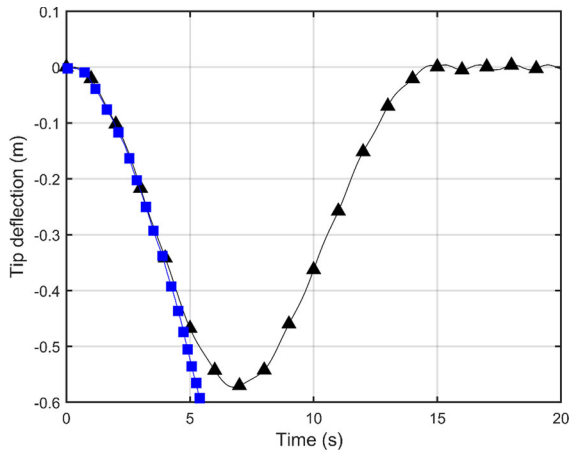

Fig. 1 Tip point deflection of the rotating beam (—▲— Nonlinear ANCF —■— Linear)

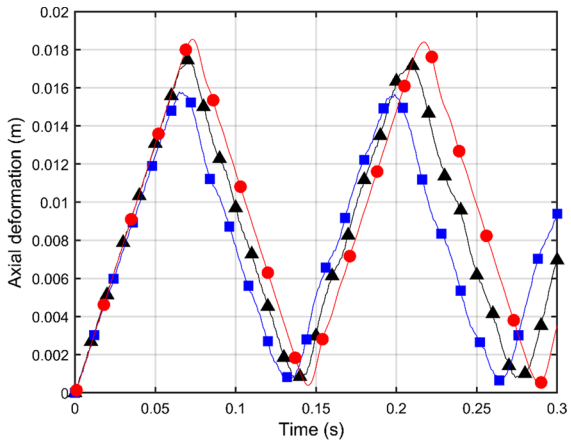

Fig. 2 Tip point axial deformation of a cantilever beam subjected to an axial force (—▲— ANCF/Plane stress, —■— ANCF/Plane strain, —●— ANSYS/BEAM188)

behavior of more general FE formulations, however, cannot always be interpreted as locking, demonstrating the need for better understanding effect of geometric stiffening and choice of constitutive models when more general formulations are used. This fact is clear from the overly stiff plane-strain results presented in Fig. 2. This overly stiff behavior is not attributed to locking, but to representation of geometric stiffening based on the constitutive model used, as will be further discussed in this investigation.

This paper addresses these fundamental problems and demonstrates that more general formulations account for deformations that are not captured by the analytical or the less general FE formulations. The limitations of the *ad hoc approaches* used in the FE literature and commercial software to account for the cross-section deformations are identified, issues associated with their inconsistency with theory of continuum mechanics are highlighted, and their appropriateness is evaluated by comparing with a more general approach. The derivation of the elastic forces using general continuum mechanics (GCM) approach, presented in this paper, is used to shed light on assumptions used in ad hoc approaches. Effects of using different constitutive models and *geometric stiffening* due to the coupling between the *cross-section deformations* and beam vibrations are studied with the goal of demonstrating that stiff behavior of more general beam formulations cannot always be interpreted as locking if convergence of the solution is achieved. Fundamental differences between classical beam approaches that assume rigid cross section, and more general beam formulations, such as the *absolute nodal coordinate formulation* (ANCF), that account for cross-section deformation are highlighted. A detailed comparative study is performed using static, dynamic, and thermal analyses to address fundamental issues related to the cross-section deformation, geometric stiffening, and locking. The obtained results are compared with results of different FE software such as ANSYS and LS-DYNA.

The paper is organized as follows. In Sect. 2, a simple example is used to define the problem addressed in this investigation and show the limitations of some beam formulations used to obtain reference solutions for the purpose of result verifications. Section 3 reviews some widely used *ad hoc approaches* used in FE formulations implemented in commercial FE software to account for cross-section deformations and identifies their limitations, which are evaluated in view of a more general formulation in Sect. 4. Geometric stiffening terms that couple different displacement modes are derived in Sect. 5 and are used to discuss limitations of the ad hoc approaches. Section 6 discusses the main difference between plane-stress and plane-strain constitutive models. Section 7 presents numerical examples used for the comparative study of this paper and demonstrates limitations of conventional FE formulations in analysis of *soft materials*. Summary and conclusions drawn from this investigation are provided in Sect. 8.

2 Problem definition

In this section, a simple beam example is used to demonstrate limitations of beam formulations, some of which are used to obtain *reference solutions* for the purpose of result verifications. The analysis presented in this section sheds light on problems associated with using analytical solutions or solutions obtained using less general FE formulations to verify numerical results obtained using more general formulations that capture deformation modes not captured by less general approaches.

2.1 Beam formulations

In order to explain the differences between different beam element formulations, a cantilever beam

subjected to an axial force $F = 10^8$ N at its free end is considered, as shown in Fig. 3. The cantilever beam has a length 1 m, height 0.3 m, and thickness 0.3 m. The material density is $\rho = 2700\,\mathrm{kg/m^3}$, while the modulus of elasticity is $E = 70 \times 10^9\,\mathrm{N/m^2}$. The Poisson ratio is varied from 0 to 0.499 to examine effect of cross-section deformation on the solution. The slenderness ratio is calculated using the equation GAl^2/EI, where G is modulus of rigidity and EI is flexural rigidity. This ratio was found to be between 44.6 and 66.7 based on the value of Poisson ratio. This ratio is greater than 30 as recommended for ANSYS BEAM188 element. Table 1 shows axial deformation predicted using different models for different Poisson ratio values when using 50 elements. Analytical solution of the axial tip deformation based on the data of the example is $\delta = Fl/EA = 0.015873$ m. The results presented in the table show that the solution predicted using the ANSYS BEAM188 element that assumes a rigid cross section is the same as the analytical solution. The deformation increases by scaling the cross section as a function of the axial elongation in ANSYS. However, the element volume is preserved to be the same after deformation as will be discussed in Sect. 3. Furthermore, the axial deformation predicted by ANSYS and LS-DYNA beam elements remains the same regardless of the value of Poisson ratio, demonstrating that the solution does not depend on Poisson ratio and some beam element formulations implemented in these two software do not account for the coupling between axial and cross-section deformations.

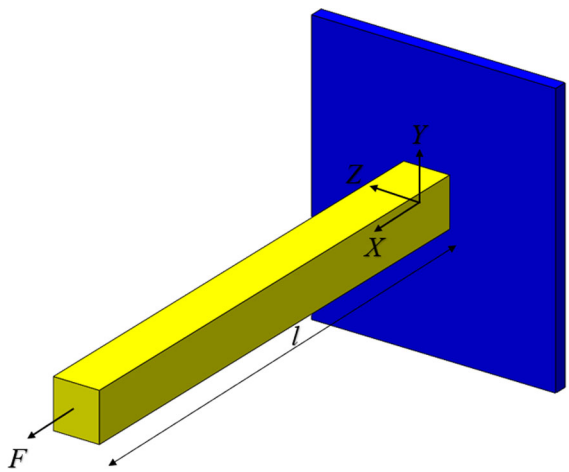

Fig. 3 Cantilever beam subjected to an axial tip force

2.2 Coupling between axial and cross-section deformations

The axial deformation becomes dependent on Poisson ratio in commercial FE software if a more general model is developed using solid (brick) elements, as demonstrated by the results presented in Table 1. The table also shows that the results obtained using the ANCF shear-deformable beam element depend on Poisson ratio because such elements automatically account for cross-section deformations. While changes in the results due to varying value of Poisson ratio are small in this example, such a Poisson effect cannot be ignored, particularly in applications in which cross-section deformation is large. It is worth mentioning that solutions obtained using commercial FE software as well as simplified analytical beam formulations are used as *reference solutions* for verification purposes. Because these reference solutions do not consider cross-section deformations and do not account for Poisson effect, it is more appropriate to use reference solutions obtained using more general formulations that were found to give solutions in agreement with experimental results [21, 25, 26].

2.3 Geometric stiffening and numerical locking

The results presented in Table 1 show that when plane-strain assumptions are used, ANCF shear-deformable beam element exhibits overly stiff behavior which can be misinterpreted as numerical locking. Such a misinterpretation can be misleading in the evaluation of the FE performance. This misinterpretation is despite the fact that elements based on more general formulations may converge to a correct solution, and such elements can have good convergence characteristics and do not suffer from locking problems.

3 Ad hoc approaches for cross-section deformations

In conventional FE beam formulations, three translational coordinates and three finite or infinitesimal rotational coordinates are used to describe, respectively, position of beam centerline and orientation of

Table 1 Tip point axial deformation for different Poisson ratio

Type	$v = 0$	$v = 0.1$	$v = 0.2$	$v = 0.3$	$v = 0.4$	$v = 0.495$
ANSYS/BEAM188/Rigid	0.015873					
ANSYS/BEAM188/Scaling	0.0162619					
ANSYS/SOLID186	0.015873	0.015858	0.015812	0.015729	0.0155998	0.015399
LS-DYNA/Belytschko–Schwer beam	0.016					
ANCF/Plane stress	0.015474	0.01546	0.01545	0.0154	0.01535	0.01529
ANCF/Plane strain	0.015474	0.01531	0.01482	0.01398	0.01278	0.01135
Analytical	0.015873					

its cross section, with assumption that the cross section does not deform [5–10]. While most beam element formulations implemented in commercial FE software employ the assumption that the cross section remains rigid, an *ad hoc approach* is used in some software to allow for cross-section deformations. The resulting displacement field in some of these formulations, however, still lacks consistency with the principles of continuum mechanics and computational geometry methods, such as B-spline and NURBS (**N**on-**U**niform **R**ational **B**-**S**pline) [27]. In this section, the *ad hoc approaches* implemented in some FE commercial software are reviewed in order to be able to explain limitations of these approaches.

3.1 Warping effect

Examples of displacement fields used in beam formulations implemented in commercial software are beam elements BEAM188 and BEAM189 implemented and recommended in software ANSYS for most beam structures. These elements, which are based on Timoshenko beam theory and capture shear effect, are suitable for modeling beam structures that are slender to moderately thick. The displacement field of the two-node BEAM188 element can be linear with one integration point, quadratic with two integration points, or cubic with three integration points. Element BEAM189, on the other hand, is a quadratic element, and it has three nodes. Each node in both elements has six degrees of freedom, three translations in x, y, and z directions, and three rotations about axes along these directions. ANSYS provides the option to increase degrees of freedom at a node from six to seven by including *warping effect* through setting the value of the parameter KEYOPT (1) to one. These elements are developed based on a first-order shear-deformation Timoshenko theory. Therefore, shear-stress variation is not allowed by these beam elements, and for this reason, *solid elements* are recommended if such a shear variation is to be considered. Poisson-ratio effect is neglected in calculation of transverse shear distribution [28]. Elements BEAM188 and BEAM189 do not account for the cross-section folding or distortion after deformation since the cross section is subjected to constant transverse shear strain. The cross section is allowed to deform in ANSYS only if the geometric nonlinearity (NLGEOM) option is considered [28].

3.2 Element Beam188

To use assumption of rigid cross section when using ANSYS BEAM188 element, parameter KEYOPT (2) is set to one. To allow for cross-section deformation as function of the axial elongation, parameter KEYOPT (2) is set to zero. This scaling option is applied only if geometric nonlinearity (NLGEOM) option is considered. However, the element volume is preserved, and this model is recommended for elastoplastic applications [28]. To ensure conservation of mass and keep constant volume for a homogenous cube subjected to an axial elongation in ANSYS, y and z transverse strains are reduced by half the axial strain, regardless of the value of Poisson ratio. In this case, the increase in volume due to axial strain is compensated by a decrease in the volume in the transverse directions to keep constant volume. This change is not physically possible for most materials that have Poisson ratio around 0.3 and also not consistent with theory of continuum mechanics that assumes that strain components are not related, particularly in case of general loading. These materials experience some increase in

the volume due to the axial elongation. The results presented in Table 1 demonstrate the limitations of this ad hoc approach that ignores effect of Poisson ratio. Another BEAM188 ad hoc approach is to use general beam cross section (GENB), which does not require providing cross-section dimensions or material properties as input data because this method utilizes data obtained experimentally or from another analysis to define the relationship between generalized stress and strain. ANSYS BEAM188 element is used in the verification study presented in this paper. This element, which is recommended for large strain, nonlinear, linear, and large rotation applications, has the nodal coordinates $\mathbf{e} = [\,u \quad v \quad w \quad \theta_x \quad \theta_y \quad \theta_z\,]^T$, where u, v, and w are the translations in the x, y, and z directions, respectively, and θ_x, θ_y, and θ_z are the rotations along axes in x, y, and z directions, respectively. The displacement field of the linear BEAM188 element, which does capture cross-section deformations, is defined as

$$\left.\begin{aligned} &u = \frac{1}{2}(u_I(1-s) + u_J(1+s)), \quad v = \frac{1}{2}(v_I(1-s) + v_J(1+s)), \\ &w = \frac{1}{2}(w_I(1-s) + w_J(1+s)), \quad \theta_x = \frac{1}{2}(\theta_{xI}(1-s) + \theta_{xJ}(1+s)), \\ &\theta_y = \frac{1}{2}(\theta_{yI}(1-s) + \theta_{yJ}(1+s)), \quad \theta_z = \frac{1}{2}(\theta_{zI}(1-s) + \theta_{zJ}(1+s)) \end{aligned}\right\} \tag{1}$$

where I and J represent the node number and s is measured along the axial direction of the beam centerline along which the integration points are defined. It is clear that beam cross-section deformation is not represented in the displacement field of this element, and cross-section deformation can be scaled as a function of the axial strain as previously discussed. The cross section of element BEAM188 is divided into subsections, and each subsection has nine nodes and four integration points. If the beam exhibits inelastic behavior along the section, constitutive computations are performed at each section integration point. Otherwise, the section pre-calculated properties at integration points along beam centerline are used [28, 29].

3.3 Solid element

Use of conventional *solid elements* to model beams can be considered as an ad hoc approach to the cross-section deformation. SOLID185 and SOLID186 are commonly used in the commercial ANSYS software. SOLID185 element has eight nodes, while SOLID186 element has twenty nodes. Each node has three degrees of freedom that are three translations in the x, y, and z directions. The displacement field is quadratic in the case of SOLID186 element, which is used in this investigation in verification studies presented in the numerical example section. The solid elements, which have more degrees of freedom than the beam elements, are recommended for thick three-dimensional solid structures. Poisson ratio effect is accounted for when using solid elements whose constitutive models are based on general continuum mechanics approach [8, 28, 29].

3.4 Belytschko–Schwer beam element

Belytschko–Schwer beam element, implemented in the FE commercial software LS-DYNA, is used with the corotational approach. This element can be used for the transient analysis of space frames that are subjected to large displacements and small strains [10, 30]. In this formulation, the deformation is defined using the element coordinates $d = [\,\delta_{IJ} \quad \theta_{xJI} \quad \theta_{yI} \quad \theta_{yJ} \quad \theta_{zI} \quad \theta_{zJ}\,]^T$, where subscripts I and J refer to node number defined at the beam ends, δ_{IJ} is the elongation, θ_{xJI} is the torsional deformation, and $\theta_{yI}, \theta_{yJ}, \theta_{zI}$, and θ_{zJ} are rotational deformations that define element bending. All rotation variables of this element are defined in local coordinate system. The displacement field of this element is defined such that the axial displacement depends linearly on element longitudinal coordinate x, while transverse displacement is cubic in x. The displacement field of this element is

$$\left.\begin{aligned} d_x^m &= (1-\xi)d_{xI} + \xi d_{xJ}, \\ d_y^m &= \left(\xi - 2\xi^2 + \xi^3\right)l\theta_{zI} + \left(-\xi^2 + \xi^3\right)l\theta_{zJ}, \\ d_z^m &= \left(-\xi + 2\xi^2 - \xi^3\right)l\theta_{yI} + \left(\xi^2 - \xi^3\right)l\theta_{yJ}, \\ \theta_x &= \xi\theta_{xJI} \end{aligned}\right\} \tag{2}$$

where $\xi = x/l$, x is measured with respect to node I, and the superscript m refers to centerline displacement. In case of Euler–Bernoulli beam, the displacement is defined as

$$\left.\begin{aligned} d_x &= d_x^m - y\left(\partial d_y^m/\partial x\right) - z\left(\partial d_z^m/\partial x\right) + H(y,z)(\partial\theta_x/\partial x) \\ d_y &= d_y^m - z\theta_x, \quad d_z = d_z^m - y\theta_x \end{aligned}\right\} \tag{3}$$

where $H(y,z)$ represents *warping function*. For this element, rigid beam cross section is assumed to be normal to beam centerline during deformation and shear effect is neglected. The strain–displacement relationships used for this element are $\varepsilon_{11} = \partial d_x/\partial x$, $\varepsilon_{12} = \left((\partial d_x/\partial y) + \left(\partial d_y/\partial x\right)\right)/2$, and $\varepsilon_{13} = ((\partial d_x/\partial z) + (\partial d_z/\partial x))/2$. The strain vector is written as $\boldsymbol{\varepsilon} = [\,\varepsilon_{11} \quad 2\varepsilon_{12} \quad 2\varepsilon_{13}\,]^T$, and matrix of strain–displacement relationships is given by

$$\mathbf{B} = \frac{1}{l}\begin{bmatrix} 1 & 0 & z(6\xi-4) & y(4-6\xi) & z(6\xi-2) & y(2-6\xi) \\ 0 & (\partial H/\partial y) - z & 0 & 0 & 0 & 0 \\ 0 & (\partial H/\partial z) - y & 0 & 0 & 0 & 0 \end{bmatrix} \tag{4}$$

It is clear that this element does not account for effect of Poisson ratio, as demonstrated by the results presented in Table 1 [10, 30]. Using the strain–displacement relationships and the stress vector $\boldsymbol{\sigma} = [\,\sigma_{11} \quad \sigma_{12} \quad \sigma_{13}\,]^T$, nodal forces can be computed using the equation $\mathbf{f} = \int_V \mathbf{B}^T\boldsymbol{\sigma}\, dV$.

4 Evaluation of ad hoc approaches

As discussed in the preceding section, the ad hoc approaches account for deformation of the cross section by enforcing a predefined relationship between transverse and axial strain components or by supplementing FE displacement field with an additional function. Supplementing the displacement field by an additional function that is not original base function of the assumed displacement field when the polynomial coefficients are replaced by the FE nodal coordinates is an ad hoc technique that is not rooted in original element geometry. Introducing predefined relationship between strains, on the other hand, is not consistent with theory of continuum mechanics that assumes that all strain components are independent and can change arbitrarily depending on the load applied to the beam.

The fact that all strain components are independent is one of the main principles used in developing ANCF finite elements [25, 26, 31–56]. Being able to replace independent assumed polynomial coefficients by gradients coordinates proves that ANCF gradient coordinates and the strains evaluated using the gradients are independent. The planar fully parameterized ANCF shear-deformable beam element can be used to evaluate assumptions of ad hoc approaches used in the FE literature and software. The global position vector $\mathbf{r}$ of an arbitrary point on this ANCF beam element can be written as $\mathbf{r}(\mathbf{x},t) = \mathbf{S}(\mathbf{x})\mathbf{e}(t)$, where $\mathbf{S}$ is element shape-function matrix, $\mathbf{x} = [\,x \quad y\,]^T$ is vector of element spatial coordinates, and $\mathbf{e}$ is vector of element nodal coordinates, which can be defined, using position vector $\mathbf{r}$ and position vector gradients $\mathbf{r}_x = \partial\mathbf{r}/\partial x$ and $\mathbf{r}_y = \partial\mathbf{r}/\partial y$, as $\mathbf{e} = \left[\,\mathbf{r}^{1T} \quad \mathbf{r}_x^{1T} \quad \mathbf{r}_y^{1T} \quad \mathbf{r}^{2T} \quad \mathbf{r}_x^{2T} \quad \mathbf{r}_y^{2T}\,\right]^T$, where the superscript refers to node number. Element shape-function matrix $\mathbf{S}(\mathbf{x})$ can be written as $\mathbf{S}(\mathbf{x}) = [\,s_1\mathbf{I} \quad s_2\mathbf{I} \quad s_3\mathbf{I} \quad s_4\mathbf{I} \quad s_5\mathbf{I} \quad s_6\mathbf{I}\,]$, where $\mathbf{I}$ is 2×2 identity matrix and shape functions s_i, $i = 1,2,\ldots,6$, are defined as [57, 58]

$$\left.\begin{aligned} s_1 &= 1 - 3\xi^2 + 2\xi^3, \quad s_2 = l\left(\xi - 2\xi^2 + \xi^3\right), \quad s_3 = l\eta(1-\xi) \\ s_4 &= 3\xi^2 - 2\xi^3, \quad s_5 = l\left(-\xi^2 + \xi^3\right), \quad s_6 = l\xi\eta \end{aligned}\right\} \tag{5}$$

where $\xi = x/l$, $\eta = y/l$, and l is the length of the element. The cross section of this element does not remain perpendicular to the neutral axis during beam deformation. Using element kinematics, global position vector $\mathbf{r}$ of an arbitrary point P, as shown in Fig. 4, can be written as $\mathbf{r} = \mathbf{r}_c + \Delta\mathbf{r} = \mathbf{r}_c + y\mathbf{r}_y$, where $\mathbf{r}_c$ is the position vector of point P_c located on the beam centerline at $y = 0$ and $\Delta\mathbf{r} = y\mathbf{r}_y$ is a vector along the beam cross section. For this ANCF element, gradient

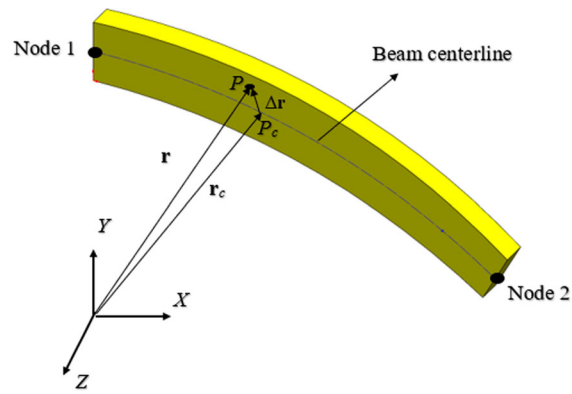

Fig. 4 Global position vector on ANCF beam element

vector $\mathbf{r}_y$, whose norm defines the change in cross-section dimensions, is linearly interpolated. That is, $\mathbf{r}_y = (1-\xi)\mathbf{r}_y^1 + \xi\mathbf{r}_y^2$, demonstrating the fact that if a geometrically consistent approach is used starting with assumed interpolating polynomials, deformation of the cross section is an integral part of the original assumed displacement field, and there is no need to supplement FE displacement field with additional functions such as $H(y,z)$, as previously discussed. The ad hoc approach in which an independent function is used to supplement FE displacement field can lead to neglect of coupling between different deformation modes.

To examine assumptions of the other ad hoc approach in which a relationship between transverse and axial strains is arbitrarily enforced, ignoring the fact that the strain components are independent, the results obtained using the ANCF beam elements for the transverse strain $\varepsilon_{22} = \left(\mathbf{r}_y^T\mathbf{r}_y - 1\right)/2$ and the axial strain $\varepsilon_{11} = \left(\mathbf{r}_x^T\mathbf{r}_x - 1\right)/2$ are obtained for the cantilever example, previously considered in this paper. These strain results are used to develop numerical representation for transverse strain ε_{22} as function of axial strain ε_{11} as $\varepsilon_{22}(\xi) = \alpha(\xi)\varepsilon_{11}(\xi)$ to see if there is certain ratio or trend in simple examples that can justify using predefined relationship between strain components to capture cross-section deformations. The scalar multiplier $\alpha(\xi)$ is plotted in Fig. 5 as function of ξ. The results presented in this figure are obtained using beam model that accounts for effect of the transverse strain on the longitudinal strain due to geometric stiffening. Such a beam model is different from models developed using cross-section scaling ad hoc approach used in commercial FE software.

As will be demonstrated in the following sections, cross-section deformation is source of *geometric nonlinearities* that can have a significant effect on stress forces. These geometric nonlinearities, as in case of the rotating blade problem, introduce *geometric stiffening* that influences amplitude of beam deformations. Geometric stiffening, which depends on the constitutive model used, may contribute to an overly stiff behavior. In case of converged FE solution, interpretation of source of higher stiffness as locking, which is associated with poor element performance, needs to be examined.

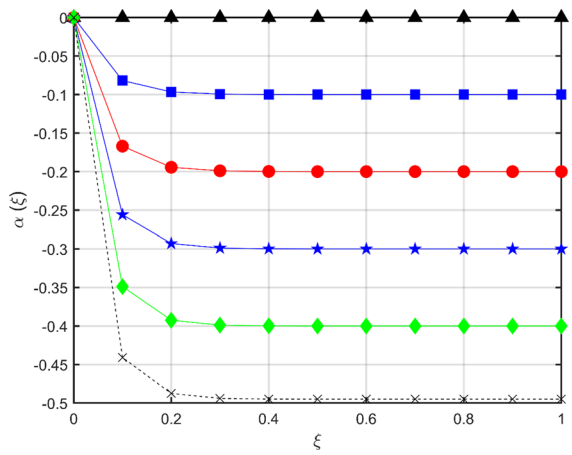

Fig. 5 The relationship between the strain components for different Poisson ratio ν (—▲—$\nu = 0$, —■—$\nu = 0.1$, —●—$\nu = 0.2$, —★—$\nu = 0.3$, —◆—$\nu = 0.4$, –x– $\nu = 0.495$)

5 Geometric nonlinearity and stiffening

In commercial FE software, four types of geometric and material nonlinearities can be considered: *large strain*, *large rotation*, *stress stiffening*, and *spin softening* [29]. Consequently, when using commercial FE software, element type and geometric nonlinearity need to be carefully selected based on the application and scope of the study. ANCF finite elements, on the other hand, automatically account for geometric nonlinearities and can describe accurately rigid-body motion including spinning at high rates without the need for using incremental co-rotation formulations. In this section, geometric nonlinearities are discussed and the terms that contribute to geometric stiffening are identified using ANCF finite elements.

5.1 Basic equations

Equation of motion of ANCF shear-deformable beam element can be written as $\mathbf{M}\ddot{\mathbf{e}} = \mathbf{Q}_e + \mathbf{Q}_s$. In this equation, $\mathbf{M} = \int_V \rho\mathbf{S}^T\mathbf{S}|\mathbf{J}_o|dV$ is the constant and symmetric element mass matrix, $\mathbf{Q}_e$ and $\mathbf{Q}_s$ are, respectively, vectors of applied and stress (elastic) forces, ρ is element mass density, V is the volume defined in the straight configuration, $|\mathbf{J}_o|$ is determinant of matrix of position gradient vectors

$\mathbf{J}_o = \partial\mathbf{X}/\partial\mathbf{x}$, $\mathbf{X} = [\,X_1 \quad X_2 \quad X_3\,]^T = \mathbf{S}\mathbf{e}_o$ defines stress-free reference configuration, $\mathbf{x} = [\,x_1 \quad x_2 \quad x_3\,]^T$ is vector of FE spatial coordinates, and $\mathbf{e}_o$ is vector of element nodal coordinates in initial reference configuration [58].

5.2 Geometric nonlinearity and cross-section deformations

Elastic forces of the ANCF beam elements can be formulated using a general continuum mechanics (GCM) approach that accounts for all nonlinear terms. In this case, strains of the planar shear-deformable ANCF beam element previously considered in this study can be written as

$$\left.\begin{aligned} \varepsilon_{11} &= \frac{1}{2}\left(\mathbf{r}_{cx}^T\mathbf{r}_{cx} - 1\right) + y\mathbf{r}_{cx}^T\mathbf{r}_{yx} + \varepsilon^{qx} \\ \varepsilon_{22} &= \frac{1}{2}\left(\mathbf{r}_y^T\mathbf{r}_y - 1\right), \quad \varepsilon_{12} = \frac{1}{2}\left(\mathbf{r}_{cx}^T\mathbf{r}_y + y\mathbf{r}_{yx}^T\mathbf{r}_y\right) \end{aligned}\right\} \tag{6}$$

where ε_{11} and ε_{22} are, respectively, axial and transverse normal strains, while ε_{12} is shear strain. Strain ε_{11} at beam centerline in axial direction x and strain ε_{22} due to cross-section stretch in transverse direction y are defined, respectively, as $(1/2)\left(\mathbf{r}_{cx}^T\mathbf{r}_{cx} - 1\right)$ and $(1/2)\left(\mathbf{r}_y^T\mathbf{r}_y - 1\right)$. The first term $(1/2)\mathbf{r}_{cx}^T\mathbf{r}_y$ in shear strain ε_{12} can be used to define shear angle at element centerline; this term may assume a nonzero value even in case of zero stretch of the cross section. The second term $y\mathbf{r}_{cx}^T\mathbf{r}_{yx}$ in normal strain ε_{11} defines the moment that produces beam bending, while third term $\varepsilon^{qx} = (1/2)y^2\mathbf{r}_{yx}^T\mathbf{r}_{yx}$ in ε_{11} represents higher-order strain components that result from cross-section deformations. It is clear that term $\varepsilon^{qx} = (1/2)y^2\mathbf{r}_{yx}^T\mathbf{r}_{yx}$ depends on gradient vector $\mathbf{r}_y$ which is an integral part of the formulation of ANCF displacement field and has influence on other strain components. Furthermore, second term $(1/2)y\mathbf{r}_{yx}^T\mathbf{r}_y$ in shear strain ε_{12} is due to cross-section deformation. It can be shown that if $\mathbf{r}_y$ remains unit vector, case of zero cross-section deformation, term $(1/2)y\mathbf{r}_{yx}^T\mathbf{r}_y$ is identically equal to zero. Terms that result from cross-section deformations couple different displacement modes, which contribute to geometric stiffening that cannot be properly captured using ad hoc approaches.

5.3 Stress force formulation

Using Eq. 6 and ANCF planar beam element kinematics, one can show that the strains can be written in terms of the nodal coordinates as

$$\left.\begin{aligned} \varepsilon_{11} &= \frac{1}{2}\left(\mathbf{e}^T\mathbf{S}_a\mathbf{e} - 1\right) + y\mathbf{e}^T\mathbf{S}_{bd}\mathbf{e} + \frac{1}{2}y^2\mathbf{e}^T\mathbf{S}_{sda}\mathbf{e} \\ \varepsilon_{22} &= \frac{1}{2}\left(\mathbf{e}^T\mathbf{S}_t\mathbf{e} - 1\right), \quad \varepsilon_{12} = \frac{1}{2}\left(\mathbf{e}^T\mathbf{S}_s\mathbf{e} + y\mathbf{e}^T\mathbf{S}_{sds}\mathbf{e}\right) \end{aligned}\right\} \tag{7}$$

In this equation, $\mathbf{S}_a = (\partial\mathbf{S}_c/\partial x)^T(\partial\mathbf{S}_c/\partial x)$, $\mathbf{S}_c = \mathbf{S}(x, y = 0)$, $\mathbf{S}_t = (\partial\mathbf{S}/\partial y)^T(\partial\mathbf{S}/\partial y)$, and $\mathbf{S}_s = (\partial\mathbf{S}_c/\partial x)^T(\partial\mathbf{S}/\partial y)$, while the functions associated with the cross section deformations are $\mathbf{S}_{bd} = (\partial\mathbf{S}_c/\partial x)^T(\partial\mathbf{S}/\partial y\partial x)$, $\mathbf{S}_{sda} = (\partial\mathbf{S}/\partial y\partial x)^T(\partial\mathbf{S}/\partial y\partial x)$, and $\mathbf{S}_{sds} = (\partial\mathbf{S}/\partial y\partial x)^T(\partial\mathbf{S}/\partial y)$. Using the strains of the preceding equations, the virtual work of the elastic forces based on the GCM approach is written in terms of the Green–Lagrange strain tensor $\boldsymbol{\varepsilon}$ and the second Piola–Kirchhoff stress tensor $\boldsymbol{\sigma}$ as $\delta W_s = -\int_V \boldsymbol{\sigma} : \delta\boldsymbol{\varepsilon}|\mathbf{J}_o|dV = \mathbf{Q}_s^T\delta\mathbf{e}$, where $\mathbf{Q}_s = -\int_V (\partial\boldsymbol{\varepsilon}/\partial\mathbf{e})^T \boldsymbol{E}\boldsymbol{\varepsilon}|\mathbf{J}_o|\mathrm{d}V$, and $\mathbf{E}$ is the elastic coefficient matrix. The definition of the stress (elastic) forces and the geometric stiffening terms depends on the constitutive model used as will be demonstrated in this paper using cases of *plane-stress* and *plane-strain constitutive models*. The plane-strain constitutive model leads to stiffer behavior, which may be wrongly interpreted as locking.

5.4 Geometric stiffening terms

Using integral expression for vector $\mathbf{Q}_s$, one can show that this nonlinear vector can be written in terms of nonlinear stiffness matrices in case of plane-strain assumptions as

$$\begin{aligned} \mathbf{Q}_s &= -((\lambda + 2\mu)\mathbf{K}_1 + \lambda\mathbf{K}_2 + 2\mu\mathbf{K}_3)\mathbf{e} \\ &= \mathbf{Q}_{s1} + \mathbf{Q}_{s2} + \mathbf{Q}_{s3} \end{aligned} \tag{8}$$

where λ and μ are Lame's constants defined as $\lambda = Ev/[(1+v)(1-2v)]$ and $\mu = E/[2(1+v)]$, E is modulus of elasticity, v is Poisson ratio, $\mathbf{Q}_{s1} = -(\lambda + 2\mu)\mathbf{K}_1\mathbf{e}$, $\mathbf{Q}_{s2} = -\lambda\mathbf{K}_2\mathbf{e}$, $\mathbf{Q}_{s3} = -2\mu\mathbf{K}_3\mathbf{e}$; and nonlinear stiffness matrixes $\mathbf{K}_1$, $\mathbf{K}_2$, and $\mathbf{K}_3$ are defined as

$$\left.\begin{aligned}\mathbf{K}_1 &= \int_V \left(\left(\frac{1}{2}\mathbf{S}_{a1} + y\mathbf{S}_{bd1} + \frac{1}{2}y^2\mathbf{S}_{sda1}\right)\varepsilon_{11} + \frac{1}{2}\mathbf{S}_{t1}\varepsilon_{22}\right)|\mathbf{J}_o|dV \\ \mathbf{K}_2 &= \int_V \left(\frac{1}{2}\mathbf{S}_{t1}\varepsilon_{11} + \left(\frac{1}{2}\mathbf{S}_{a1} + y\mathbf{S}_{bd1} + \frac{1}{2}y^2\mathbf{S}_{sda1}\right)\varepsilon_{22}\right)|\mathbf{J}_o|dV \\ \mathbf{K}_3 &= \frac{1}{2}\int_V ((\mathbf{S}_{s1} + y\mathbf{S}_{sds1})\varepsilon_{12})\,|\mathbf{J}_o|dV\end{aligned}\right\} \tag{9}$$

where $\mathbf{S}_{a1} = \mathbf{S}_a + \mathbf{S}_a^T$, $\mathbf{S}_{bd1} = \mathbf{S}_{bd} + \mathbf{S}_{bd}^T$, $\mathbf{S}_{sda1} = \mathbf{S}_{sda} + \mathbf{S}_{sda}^T$, $\mathbf{S}_{t1} = \mathbf{S}_t + \mathbf{S}_t^T$, $\mathbf{S}_{s1} = \mathbf{S}_s + \mathbf{S}_s^T$, and $\mathbf{S}_{sds1} = \mathbf{S}_{sds} + \mathbf{S}_{sds}^T$. The stiffness matrices in the preceding equation have coupling terms between the element coordinates that cannot be captured using ad hoc approaches. This stiffness coupling produces geometric stiffening that can be important in large-deformation applications. Linearization approaches that neglect geometric stiffening terms, as in case of rotor blade benchmark example, can lead to wrong solutions and misleading information on system stability. This issue is particularly important in large-deformation analysis and in analysis of soft robots and materials [59].

6 Constitutive models

In order to examine the effect of the constitutive models and have proper interpretation of stiff beam behavior, the two cases of *plane-strain* and *plane-stress* constitutive models are considered. In case of linear elastic model, stresses can be written in terms of strains using constitutive equation $\boldsymbol{\sigma} = \mathbf{E}\boldsymbol{\varepsilon}$. The matrix of elastic coefficient $\mathbf{E}$ in case of plane strain is

$$\mathbf{E} = \begin{bmatrix} \lambda + 2\mu & \lambda & 0 \\ \lambda & \lambda + 2\mu & 0 \\ 0 & 0 & 2\mu \end{bmatrix} \tag{10}$$

In this case, $\varepsilon_{13} = \varepsilon_{23} = \varepsilon_{33} = 0$, and the stresses are given by

$$\left.\begin{aligned}&\sigma_{11} = (\lambda + 2\mu)\varepsilon_{11} + \lambda\varepsilon_{22}, \quad \sigma_{22} = (\lambda + 2\mu)\varepsilon_{22} + \lambda\varepsilon_{11}, \\ &\sigma_{33} = \lambda(\varepsilon_{11} + \varepsilon_{22}), \quad \sigma_{12} = 2\mu\varepsilon_{12}\end{aligned}\right\} \tag{11}$$

In case of plane-strain assumption, the deformation or strain is restricted in the thickness direction, and the strain is zero in the Z direction. Consequently, there is a stress in the thickness direction. The plane-strain assumption is often applied in case of thick structures.

On the other hand, the matrix $\mathbf{E}$ in case of plane-stress assumption can be written as

$$\mathbf{E} = E\begin{bmatrix} 1/(1-\nu^2) & \nu/(1-\nu^2) & 0 \\ \nu/(1-\nu^2) & 1/(1-\nu^2) & 0 \\ 0 & 0 & 1/(1+\nu) \end{bmatrix} \tag{12}$$

In this case, $\sigma_{13} = \sigma_{23} = \sigma_{33} = 0$, and the strains are given by

$$\left.\begin{aligned}&\varepsilon_{11} = (\sigma_{11} - \nu\sigma_{22})/E, \quad \varepsilon_{22} = (\sigma_{22} - \nu\sigma_{11})/E, \\ &\varepsilon_{33} = -\nu(\sigma_{11} + \sigma_{22})/E, \quad \varepsilon_{12} = ((1+\nu)/E)\sigma_{12}\end{aligned}\right\} \tag{13}$$

The plane stress assumes that the stress along the Z direction is zero, but the strain in the thickness direction is not zero because of Poisson effect, and the deformation in Z direction is not restricted. The plane-stress assumption is recommended for thin structures.

Figure 6 shows a cantilever beam that has restrictions on the outer surfaces to prevent cross-section expansion in the transverse directions. A cross-section stretch due to Poisson effect is prevented because of the outer-surface constraint. Consequently, the developed residual normal transverse stress σ_{33} contributes to the axial strain according to the equation $\varepsilon_{11} = (\sigma_{11} - \nu(\sigma_{22} + \sigma_{33}))/E$. In this case, plane-strain assumption is more appropriate because

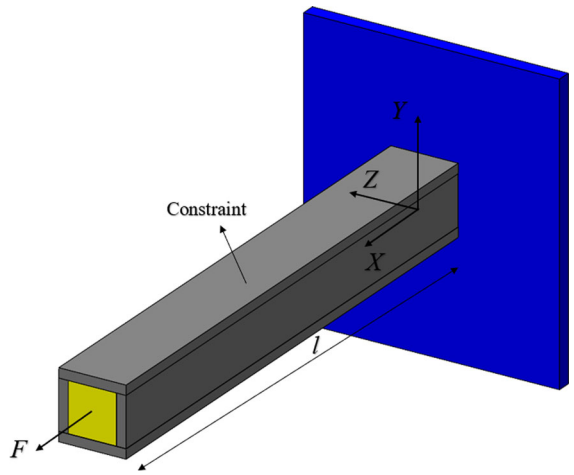

Fig. 6 Cantilever beam subjected to an axial tip force and displacement constraints

deformation in the thickness direction is restricted, while the stress in the thickness direction is not zero. On the other hand, the strain in the thickness direction ε_{33} is nonzero in case of plane-stress assumption, and there is no stress in the thickness direction. Using assumption of plane stress in this example leads to inaccurate results because axial strain does not account for the developed residual normal stress σ_{33} that cannot be ignored in this case. In general, the plane stress is recommended in most cases if the beam thickness does not exceed the beam length. However, if there are constraints on the outer surfaces to prevent the transverse deformation as shown in Fig. 6, then the plane strain is recommended. The numerical examples presented in the following section will demonstrate the difference between results obtained using the two constitutive models. These results explain the stiff behavior exhibited in some plane-strain models and demonstrate that such a stiff behavior should not always be interpreted as locking [12, 60–65].

7 Numerical examples

Several numerical examples are used in this section to study effect of using different constitutive models. Static, dynamic, and thermal analyses are performed to discuss effect of constitutive models on beam stiffness. The results obtained using general-purpose MBS software **SIGMA/SAMS** (**S**ystematic **I**ntegration of **G**eometric **M**odeling and **A**nalysis for the **S**imulation of **A**rticulated **M**echanical **S**ystems) are compared with results of commercial FE software ANSYS and LS-DYNA.

7.1 Static analysis

The first example is a cantilever beam connected to a frame using fully-clamped joint, as shown in Fig. 3. The clamped joint eliminates all rigid-body and deformation degrees of freedom at the end connected to the frame. The material and geometric properties of the cantilever beam are the same as the properties provided in Sect. 2.1 with the exception that Poisson ratio is selected to be 0.3. Table 2 compares numerical solutions obtained using SIGMA/SAMS, ANSYS, and LS-DYNA software. BEAM188 is used in ANSYS, while Belytschko–Schwer beam with full cross-section integration is used in LS-DYNA. Using the assumption of cross-section scaling in ANSYS leads to results that are close to LS-DYNA, and these results are higher than the analytical solution. This is despite the fact that in case of rigid cross section, all energy is consumed by the axial deformation, while in case of deformable cross section, part of energy is consumed in the cross-section deformation. This is not achieved in case of cross-section scaling in ANSYS as shown in Table 2 because the element volume is preserved as discussed before. The results presented in Table 2 show that there is no significant difference between the solution in case of zero Poisson ratio and ANCF plane-stress solution. Poisson effect is not captured by the analytical solution or the less general beam elements in commercial FE software as previously discussed. Furthermore, when the strain split method (SSM) is used for locking alleviation [12, 65], the same results are obtained for plane-strain and plane-stress constitutive models. The results presented in Table 2 demonstrate that the stiff behavior of the plane-strain model cannot be interpreted as locking, but to the choice of the constitutive model.

Table 2 Axial deformation of the cantilever beam subjected to an axial tip force

Type	5 elements	10 elements	20 elements	50 elements
ANCF/Plane strain	0.0136687	0.013852429	0.013936282	0.013980346
ANCF/Plane stress	0.01506538	0.015257183	0.015348306	0.015400819
ANCF/Zero Poisson ratio	0.015141531	0.015325914	0.015418095	0.015474461
LS-DYNA/Belytschko–Schwer beam	0.016	0.016	0.016	0.016
ANSYS/BEAM188/Rigid	0.015873	0.015873	0.015873	0.015873
ANSYS/BEAM188/Scaling	0.0162619	0.0162619	0.0162619	0.0162619
Analytical	0.015873			

The second example considered in this section is the same as the first example, but the outer surfaces are constrained to prevent the transverse deformations as shown in Fig. 6. In this case, three-dimensional elements are used in ANSYS and LS-DYNA to apply constraints on the outer surfaces. These constraints cannot be applied to the beam elements in commercial FE software because Poisson effect is not considered. While the option of general beam cross section (GENB) can be used in ANSYS BEAM188 to represent cross-section deformation, this element formulation requires relation between the stress and strain that has to be determined using another method. For this reason, ANSYS element SOLID186 that has twenty nodes is used, while fully integrated quadratic 8-node solid element with nodal rotations is used in LS-DYNA. In case of ANCF model, position vector gradient $\mathbf{r}_y$ of each node is constrained to be $\mathbf{r}_y = [0 \quad 1]^T$.

Table 3 shows calculated static axial deformation of the cantilever beam with transverse deformation constraints using different software. ANCF plane-strain solution is approximately the same as ANSYS and LS-DYNA solutions for this model. ANCF plane-stress solution is different from ANSYS and LS-DYNA solutions due to assumption of zero stress in the thickness direction as previously discussed. Clearly, the plane-strain assumption is more consistent with constraints imposed on the transverse deformation. The results also show that use of zero Poisson ratio leads to the same results as those obtained in the first example. Therefore, the constitutive model should be properly selected to obtain accurate results and avoid misinterpretation of stiff behaviors as locking.

7.2 Vibration problems

Effect of choice of the constitutive model on a *cantilever beam* made of soft material is examined in this section. Dimensions of the beam are the same as dimensions of the model previously used in this section. However, soft material with modulus of elasticity $E = 1.2 \times 10^6 \mathrm{N/m}^2$, mass density $\rho = 1500\,\mathrm{kg/m}^3$, and Poisson ratio $v = 0.3$ is used [66]. The beam is subjected to an axial tip force $F = 1000\cos(5\pi t)$, and effect of gravity is neglected. Twelve ANCF beam elements are used in this example, and the results are compared with solutions obtained using BEAM188 in ANSYS and Belytschko–Schwer beam in LS-DYNA. Figure 7 compares axial deformation predicted using different software in case of beam that does not have any cross-section deformation constraints. It is shown that ANCF plane-stress solution agrees well with ANSYS and LS-DYNA solutions, while plane-strain

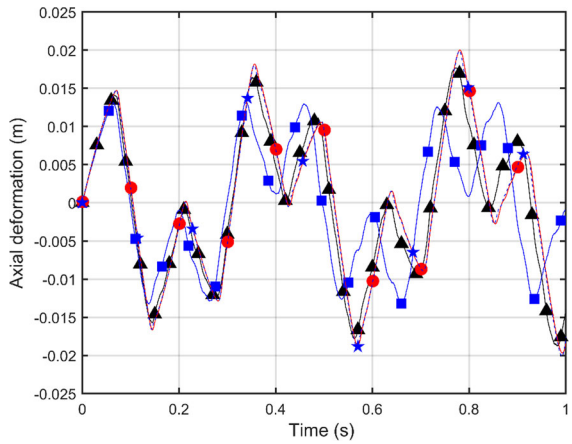

Fig. 7 Tip point axial deformation of the cantilever beam subjected to a harmonic axial force (—▲— ANCF/Plane stress, —■— ANCF/Plane strain, —●— ANSYS/BEAM188, – –★– – LS-DYNA/Belytschko–Schwer beam)

Table 3 Axial deformation of the cantilever beam subjected to an axial tip force and transverse displacement constraints

Type	5 elements	10 elements	20 elements	50 elements
ANCF/Plane strain	0.011314191	0.011451667	0.011520405	0.011562188
ANCF/Plane stress	0.013806984	0.013974984	0.014059004	0.014110425
ANCF/Zero Poisson ratio	0.015141531	0.015325914	0.015418095	0.015474461
LS-DYNA/Quadratic solid	0.01192			
ANSYS/SOLID186	0.0117914			

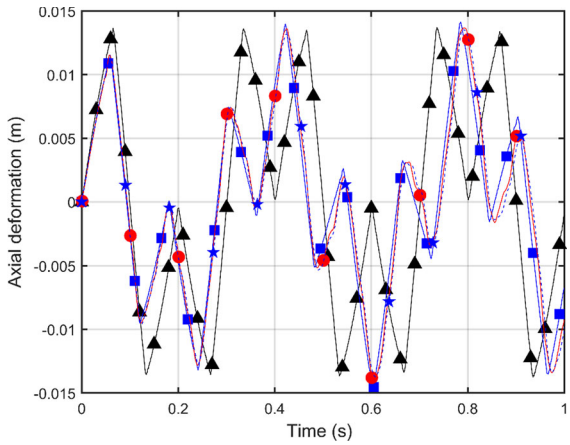

Fig. 8 Tip point axial deformation of the cantilever beam subjected to a harmonic axial tip force and displacement constraints (—▲— ANCF/Plane stress, —■— ANCF/Plane strain, —●— ANSYS/SOLID186, – –★– – LS-DYNA/Quadratic Solid)

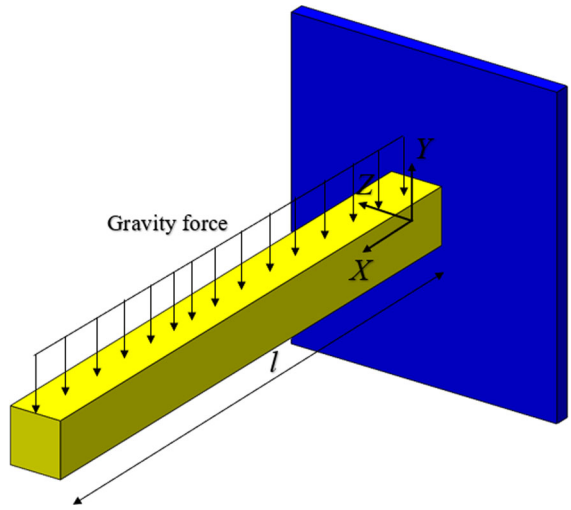

Fig. 9 Cantilever beam under the gravity effect

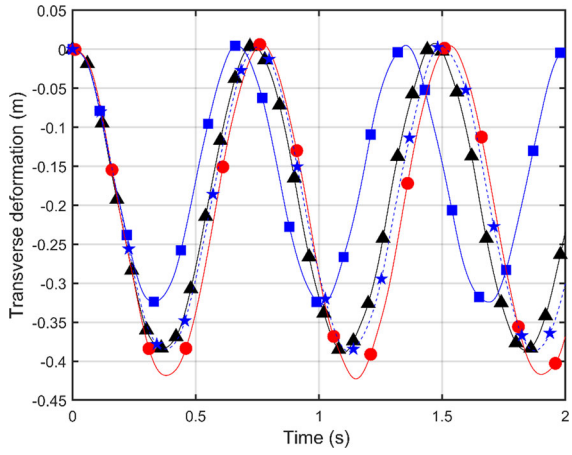

Fig. 10 Tip point vertical deformation of the cantilever beam under the gravity effect (—▲— ANCF/Plane stress —■— ANCF/Plane strain, —●— ANSYS/BEAM188, – –★– – LS-DYNA/Belytschko–Schwer beam)

assumption leads to different results. In case of constraining outer surfaces, as shown in Fig. 6, element SOLID186 is used in ANSYS, while fully integrated quadratic 8-node solid element is used in LS-DYNA. Figure 8 shows that ANCF plane-strain axial deformation solution is close to ANSYS and LS-DYNA solutions, while plane-stress solution is different from ANSYS and LS-DYNA.

A second example of a cantilever beam falling under gravity effect, as shown in Fig. 9, is considered. The dimensions and material properties of the cantilever beam are the same as the previous example. The tip transverse deformation using different formulations is presented in Fig. 10, which shows that plane-strain solution has lower amplitudes compared to ANSYS and LS-DYNA solutions. The plane-stress solution agrees well with LS-DYNA solution and slightly differs from solution of ANSYS BEAM188 element, which is based on Timoshenko beam theory that accounts for the shear effect. This effect is significant in this example because the beam slenderness ratio is greater than 50. The implementation of the Belytschko–Schwer beam in LS-DYNA is based on the corotational approach, and it gives results close to Euler–Bernoulli beam. Because ANCF beam cross-section stretch is allowed, part of the energy contributes to the cross-section deformation. Poisson effect is considered in ANCF beam element, while it is ignored in axial beam element problems in commercial FE software, as previously discussed. It should be mentioned that the analytical vertical tip deflection in case of cantilever beam subjected to a vertical tip force is affected by Poisson ratio in case of BEAM188 because formulation of this element is based on Timoshenko beam theory. In this case, the vertical tip displacement according to Timoshenko is given by $\delta_y = (F/6EI)\left[(4+5\nu)\left(w^2 l/4\right) + 2l^3\right]$ [2]. However, this does not mean that cross-section

deformation is considered; Timoshenko theory considers cross-section rotation due to shear, while the analytical solution of the vertical tip deformation using Belytschko–Schwer beam gives results close to Euler–Bernoulli beam solution calculated by $\delta_y = FL^3/3EI$. These results are not affected by changing Poisson ratio.

7.3 Dynamic problems

While solutions of ANCF and FE conventional formulations can have a good agreement in case of structural small-deformation problems, there can be differences between these solutions in case of large displacements. Recent investigations have addressed this issue in case of soft materials that have large deformations [25, 26]. To investigate this issue, two pendulum beams made of stiff and soft materials are considered. The pendulum is connected at one end to the ground by a revolute joint, while the other end is free as shown in Fig. 11. The beam, initially horizontal with zero initial velocity, falls under gravity effect. The beam is assumed to have length 1.2 m, height 0.25298 m, and width 0.00632 m. In the first case considered, stiff material, with modulus of elasticity $E = 2 \times 10^{11}\mathrm{N/m^2}$, mass density $\rho = 7800\,\mathrm{kg/m^3}$, and Poisson ratio $\nu = 0.3$, is used. Figure 12, which compares the vertical tip displacement predicted using ANCF (12 elements), ANSYS (BEAM188), and LS-DYNA (Belytschko–Schwer beam) models, shows that the ANCF plane stress, ANCF plane strain,

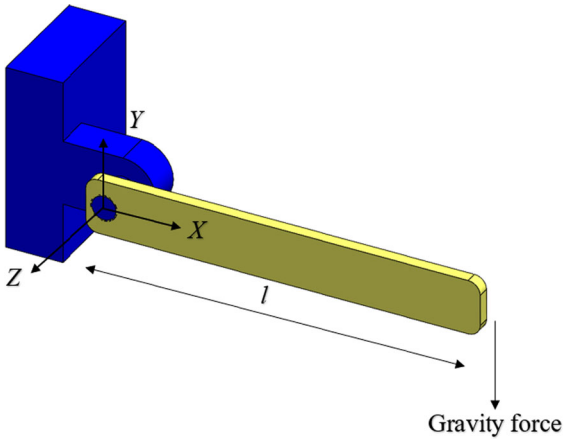

Fig. 11 Free-falling planar pendulum

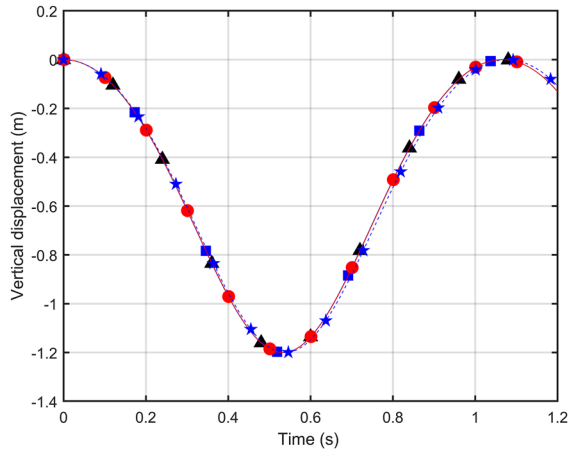

Fig. 12 Tip point vertical displacement of the stiff free-falling planar pendulum (—▲— ANCF/Plane stress —■— ANCF/Plane strain, —●— ANSYS/BEAM188, - -★- - LS-DYNA/Belytschko–Schwer beam)

ANSYS (BEAM188), and LS-DYNA (Belytschko–Schwer beam) solutions are in a good agreement. These results demonstrate that ANCF and FE conventional formulations agree well in case of small deformation.

In order to examine effect of the constitutive models and use of the FE software in the case of soft materials, model parameters are changed to $E = 0.7 \times 10^6\mathrm{N/m^2}$, $\rho = 5540\mathrm{kg/m^3}$, and $\nu = 0.3$ [57]. Figure 13 shows a good agreement between the

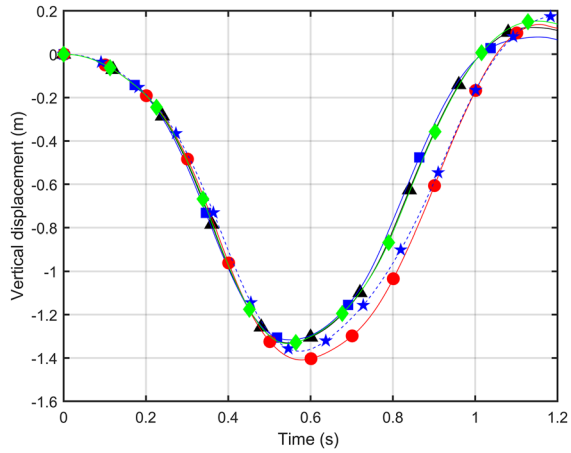

Fig. 13 Tip point vertical displacement of the soft free-falling planar pendulum (—▲— ANCF/Plane stress —■— ANCF/Plane strain, —●— ANSYS/BEAM188, - -★- - LS-DYNA/Belytschko–Schwer beam, —◆— ANCF/GCM/SSM)

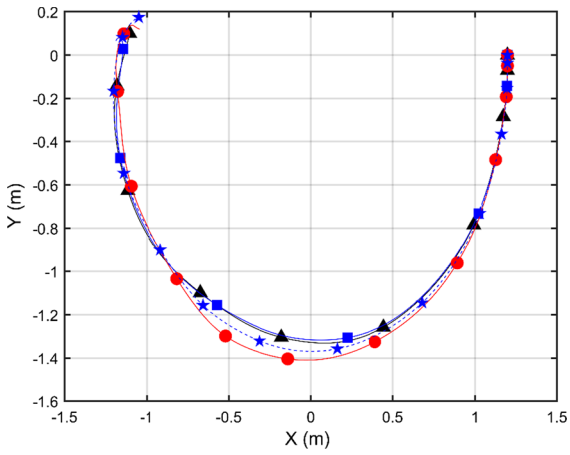

Fig. 14 Tip point position of the soft free-falling planar pendulum (—▲— ANCF/Plane stress —■— ANCF/Plane strain, —●— ANSYS/BEAM188, --★-- LS-DYNA/Belytschko–Schwer beam)

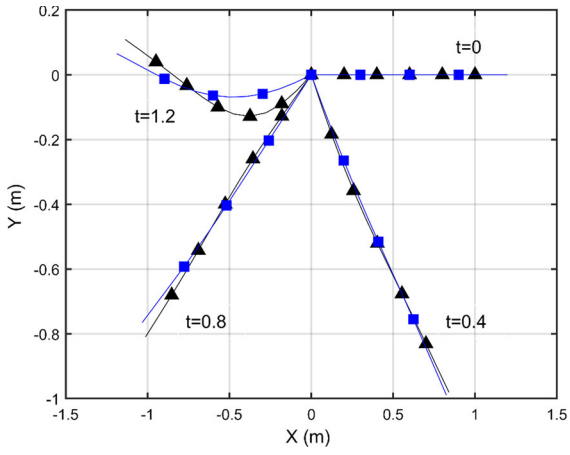

Fig. 15 Free-falling planar pendulum at different time points (—▲— ANCF/Plane stress —■— ANCF/Plane strain)

plane stress solution and solution obtained using the GCM/SSM, recently introduced for locking alleviation based on modification of the constitutive model. These results demonstrate that proper choice of the constitutive model can alleviate need for using locking alleviation techniques in some applications. Figure 13 and the results presented in Fig. 14 confirm concerns regarding using conventional FE methods and software in analysis of soft material large deformations. Figure 15, which depicts pendulum shape at different time points for plane-strain and plane-stress cases, shows that the beam behaves more flexible in plane-stress case.

7.4 Mechanism system

The planar slider crank mechanism shown in Fig. 16 consists of four bodies: ground, crankshaft, connecting rod, and slider block. The ground is connected to the crankshaft by a revolute joint at point O and to the slider by a prismatic joint. The crankshaft is connected to the connecting rod by a revolute joint at point A, and the connecting rod is connected to the slider block by a revolute joint at point B. The bodies are assumed in the horizontal position in the initial configuration. The slider block has zero mass, and effect of gravity is neglected for all bodies. The crankshaft has length 0.152 m, cross-sectional area $7.854 \times 10^{-5}\mathrm{m}^2$, second moment of area $4.909 \times 10^{-10}\mathrm{m}^4$, and mass density $\rho = 2770\mathrm{kg}/\mathrm{m}^3$. The connecting rod length is 0.304 m, while its cross-section area and mass density are the same as the crankshaft. The modulus of elasticity of the connecting rod is selected to be $E = 0.5 \times 10^8\mathrm{N}/\mathrm{m}^2$. All bodies are assumed rigid except the connecting rod, which is considered flexible and modeled using eight planar ANCF elements. The driving moment applied to the crankshaft is defined as follows:

$$M(t) = \begin{cases} 0.01\left(1 - e^{-(t/0.167)}\right) & t < 0.7s \\ 0 & t \geq 0.7s \end{cases} \tag{14}$$

This mechanism example is also solved using the *floating frame of reference* (FFR) formulation. Figure 17, which shows the connecting rod midpoint transverse deformation using different formulations, demonstrates effect of using different constitutive models. The plane-stress solution agrees with FFR and ANCF solutions that assume zero Poisson ratio, while the plane-strain solution differs from other solutions.

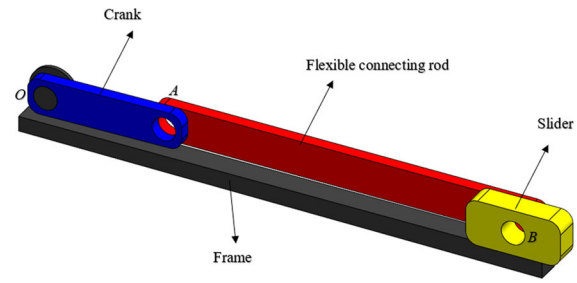

Fig. 16 Slider crank mechanism with flexible connecting rod

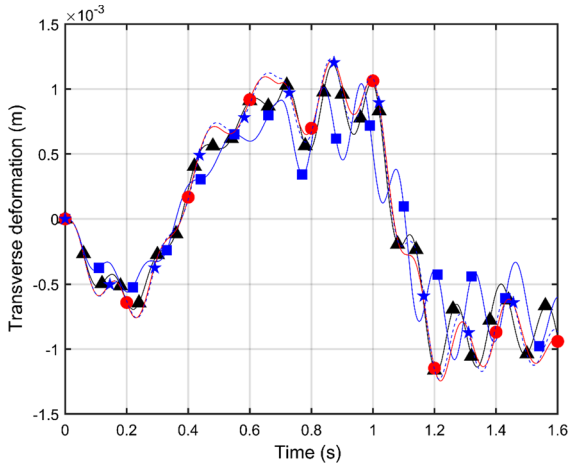

Fig. 17 Midpoint transverse deformation of the connecting rod (—▲— ANCF/Plane stress —■— ANCF/Plane strain, —●— ANCF/Zero Poisson ratio, – –★– – FFR)

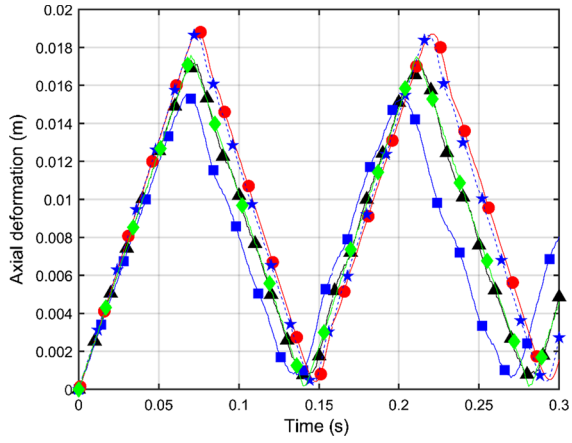

Fig. 18 Tip point axial deformation of the cantilever beam in the case of thermal expansion (—▲— ANCF/Plane stress —■— ANCF/Plane strain, —◆— ANCF/Zero Poisson ratio, —●— ANSYS/BEAM188, – –★– – LS-DYNA/Belytschko–Schwer beam)

7.5 Thermal analysis

Thermal analysis is performed in this section to investigate effect of using assumptions of rigid and deformable beam cross sections. A cantilever beam with length 1 m and square $0.3 \times 0.3\,\mathrm{m}^2$ cross section is used. The beam is made of soft material with modulus of elasticity $E = 1.2 \times 10^6\ \mathrm{N/m}^2$, Poisson ratio $v = 0.3$, and mass density $\rho = 1500\,\mathrm{kg/m}^3$. Constant thermal load is applied to the beam; and coefficient of thermal expansion is assumed $\alpha_\Theta = 0.0001\ (1/^\circ\mathrm{C})$. The beam is subjected to temperature change $\Delta\Theta = 200^\circ\mathrm{C}$. Due to thermal effect, vector of element nodal coordinates is changed to account for thermal expansion $\alpha_\Theta\Delta\Theta$. New vector of element nodal coordinates for one ANCF element that accounts for thermal expansion can be written as follows [67]:

$$\mathbf{e}^1_{o+\Theta} = [0\ \ 0\ \ 1+\alpha_\Theta\Delta\Theta\ \ 0\ \ 0\ \ 1+\alpha_\Theta\Delta\Theta]^T$$
$$\mathbf{e}^2_{o+\Theta} = [l(1+\alpha_\Theta\Delta\Theta)\ \ 0\ \ 1+\alpha_\Theta\Delta\Theta\ \ 0\ \ 0\ \ 1+\alpha_\Theta\Delta\Theta]^T \quad (15)$$

Furthermore, 1000 N axial force is applied to the tip of the cantilever beam, while effect of gravity is neglected. The problem is solved using ANCF (12 elements), ANSYS (BEAM188), and LS-DYNA (Belytschko–Schwer beam) by applying thermal load at a preprocessor step, and the new deformed shape is subjected to the axial tip force. Figure 18 shows ANCF, ANSYS, and LS-DYNA solutions of the tip point axial deformation. The results show a noticeable difference between ANCF plane-strain and conventional FE solutions, while plane-stress solution and zero Poisson ratio solution agree well with ANSYS and LS-DYNA solutions. This slight difference between plane-stress and FE software solutions can be attributed to assumption of rigid cross section in conventional FE models; this assumption is relaxed in ANCF model. The ANSYS and LS-DYNA results remain the same by changing length of the beam due to the thermal expansion to 1.02 m and using cross-section dimensions $0.3 \times 0.3\,\mathrm{m}^2$. Figure 19 shows the difference between the undeformed and deformed configurations using ANCF elements, and conventional beam elements of ANSYS and LS-DYNA. The results of this figure explain the concerns regarding use of FE commercial software beam elements that consider rigid cross section that is not sensitive to thermal load. It was found that using ANSYS cross-section scaling method based on the axial elongation has no significant effect on the results in this case. To further investigate this issue, the problem is solved using ANSYS SOLID186 element which accounts for cross-section expansion due to thermal load. Also, ANSYS BEAM188 and LS-DYNA Belytschko–Schwer beam that employ ad hoc approaches to account for cross-section deformations are also considered with cross-section dimensions of both beam elements

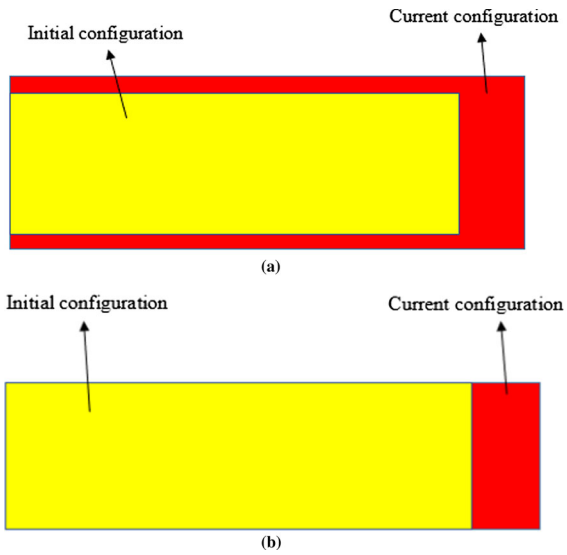

Fig. 19 Effect of the thermal expansion on the straight beam using different formulations: **a** ANCF and **b** BEAM188 and Belytschko–Schwer beam

changed manually to $0.306 \times 0.306\,\mathrm{m}^2$ and length changed to 1.02 m to account for thermal expansion effect. Figure 20 shows that ANCF plane-stress solution agrees with ANSYS and LS-DYNA beam solutions that employ ad hoc approaches. The results of this figure also show that solid elements account for thermal load cross-section expansion without the need for an ad hoc approach. However, solid elements are not suited, in general, for solving beam bending problems, and for this reason, having accurate and general beam formulations is necessary.

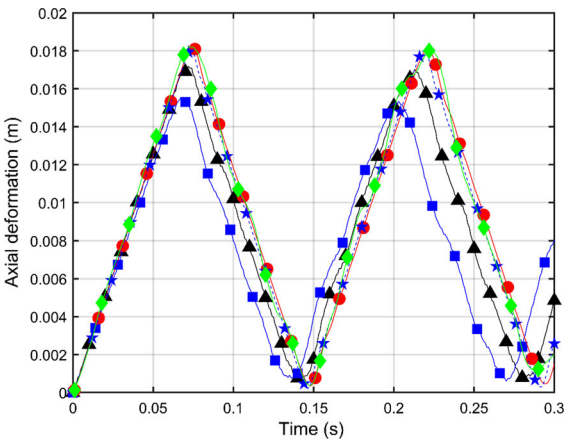

Fig. 20 Tip point axial deformation of the cantilever beam in the case of thermal expansion and cross-section adjustment (—▲— ANCF/Plane stress —■— ANCF/Plane strain, —●— ANSYS/BEAM188, —◆— ANSYS/SOLID186, – –★– – LS-DYNA/Belytschko–Schwer beam)

7.6 Rotating planar beam

Geometric stiffening resulting from coupling between different modes of displacements can influence the solutions in different ways. Coupling between cross-section deformation and axial and bending deformations is one example. Another example is axial/bending deformation coupling which has been an issue in field of rotor dynamics. The geometric stiffening effect, as result of axial/bending deformation coupling, has been investigated using rotating beam problems, which demonstrated that linearization of equations of motion can lead to misleading stability results, as demonstrated by the results presented in Fig. 1. While in some conventional beam formulations, measures must be taken to ensure properly accounting for effect of geometric stiffening, no such measures are required using ANCF elements that employ GCM approach for formulation of stress forces. Figure 21 shows a planar beam rotating about the vertical Z-axis with an angular velocity Ω. The beam, assumed initially horizontal, has length 10 m, cross-section area $4 \times 10^{-4}\,\mathrm{m}^2$, second moment of area $2 \times 10^{-7}\,\mathrm{m}^4$, mass density 3000 kg/m^3, modulus of elasticity 7×10^{10} Pa, and Poisson ratio 0.3 [22]. Effect of gravity is neglected, initial velocity is zero, and angular rotation profile is defined by the equation

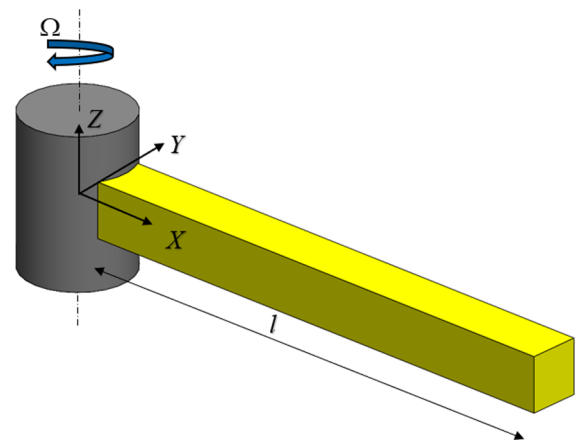

Fig. 21 Rotating beam

$$\theta(t) = \begin{cases} \frac{\Omega}{T}\left\{\frac{t^2}{2} + \left(\frac{T}{2\pi}\right)^2\left[\cos\left(\frac{2\pi t}{T}\right) - 1\right]\right\}, & t < T \\ \Omega\left(t - \frac{T}{2}\right), & t \geq T \end{cases} \tag{16}$$

where $T = 15$ s, $\Omega = 6$ rad/s, and after $t = T$, the angular velocity remains constant. The simulation time is assumed 20 s. Sixteen ANCF elements are used in the analysis of this example, which has been a benchmark example in many investigations, most of which assume zero Poisson ratio [20–24]. Nonetheless, all previous investigations demonstrated that linearization that does not account for geometric stiffening leads to unstable solution which is not supported by experimental observations. Figure 22 shows that the tip point deflection predicted using all models oscillates in the steady state around the zero value with a small amplitude. The zero Poisson ratio solution does not account for geometric stiffening resulting from deformation of the cross section, but it properly accounts for geometric stiffening resulting from axial/bending deformation coupling, which is more significant in this problem. Plane-stress and plane-strain solutions, on the other hand, account for both types of coupling.

7.7 Nonlinear constitutive model

In this investigation, linear Hookean model was used to study effect of using different linear constitutive models such as plane stress and plane strain. However, there are nonlinear constitutive models that can be used with soft materials such as compressible Neo-Hookean and the incompressible Mooney–Rivlin. The results of linear and nonlinear constitutive models were found to be in good agreement in case of small deformations, while differences were observed in case of large deformation [68]. Figures 23 and 24 compare between the tip point vertical displacement and midpoint transverse deformation of the soft pendulum discussed in Sect. 7.3 using linear Hookean and nonlinear compressible Neo-Hookean. It is shown that there is a slight difference between results of

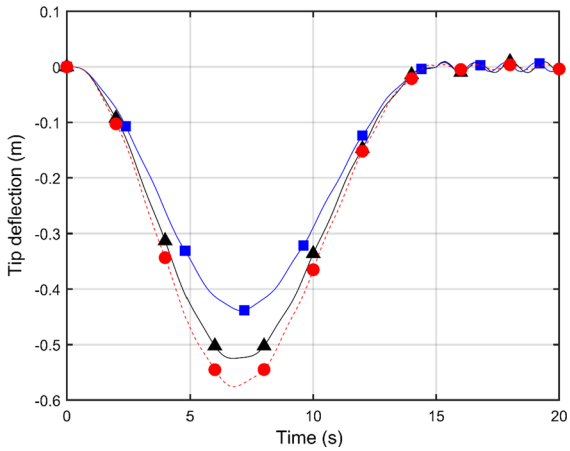

Fig. 22 Tip point transverse deflection of the rotating beam (—▲— ANCF/Plane stress, —■— ANCF/Plane strain, – – –●– – – ANCF/Zero Poisson ratio)

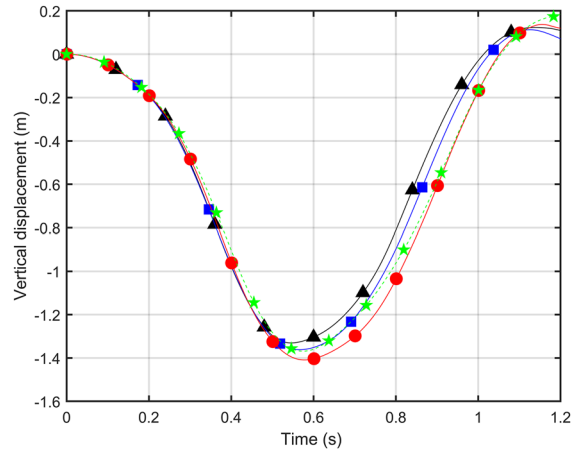

Fig. 23 Tip point vertical displacement of the soft free-falling planar pendulum (—▲— ANCF/Hookean —■— ANCF/Neo-Hookean, —●— ANSYS/BEAM188, —★— LS-DYNA/Belytschko–Schwer beam)

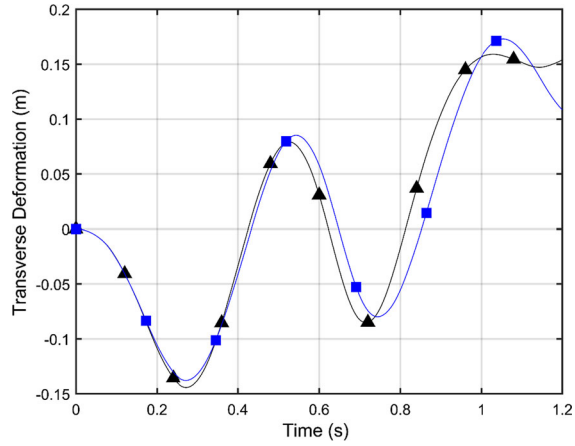

Fig. 24 Midpoint transverse deformation of the soft free-falling planar pendulum (—▲— ANCF/Hookean —■— ANCF/Neo-Hookean)

linear and nonlinear constitutive models. These results are still different from ANSYS and LS-DYNA results in case of soft material as previously discussed.

8 Conclusions

The stiff behavior of more general FE beam formulations can be wrongly interpreted as *locking* in some problems such as axial problems based on comparing with the results obtained using analytical and/or less general FE beam formulations that employ simplifying assumptions. The analysis and results obtained in this paper demonstrate that more general FE beam formulations can lead to higher stiffness attributed to *geometric nonlinearities* resulting from cross-section deformations. Such modes of deformation are not properly captured by analytical or less general FE beam formulations. Furthermore, the high stiffness exhibited by solutions based on formulations that account for these deformation modes may not, in general, be interpreted as locking. Limitations of *ad hoc approaches* used in conventional FE beam formulations implemented in commercial FE software to account for beam cross-section deformations are discussed, and their inconsistency with theory of continuum mechanics is highlighted. Relation between geometric stiffening, cross-section deformation, locking, and constitutive model in more general FE beam formulations is explained. It is shown that use of different constitutive models, such as plane stress and plane strain, can lead to different degrees of stiffness for the same element, a result that needs to be considered for proper evaluation of FE performance. Several numerical examples are used to perform static, dynamic, and thermal analyses; and results obtained are compared with FE commercial software such as ANSYS and LS-DYNA. Limitations of ad hoc approaches implemented in commercial software to account for deformation of the cross section are discussed. Such ad hoc approaches are not rooted in Bezier or computational geometry methods. Numerical results obtained in this paper shed light on problems of using simplified analytical solutions for verification of solutions and provide justifications for concerns raised regarding use of conventional FE approaches in analysis of soft robots and materials.

While the analysis and conclusions of the paper with regard to geometric stiffening, interpretation of locking, and coupling between different modes were based on a planar analysis, three-dimensional analysis can be performed in future investigation to have an understanding of effect of geometric stiffening and to properly interpret locking effect. In a three-dimensional analysis, more cross-section deformation modes must be considered [69]. Furthermore, more studies are needed to understand warping effect and its coupling with axial and bending deformations of beams. For such studies, higher-order interpolation of cross-section deformation may be necessary to accurately represent a more general cross-section deformed shape. Linear interpolation of the gradient vectors allows for only capturing cross-section stretch. Future investigations will also shed light on whether simplified beam models that assume constant cross section can be used for purpose of reliable result verification and whether coupled deformation modes which are not captured using these simplified models can yield accurate results in more general vibration and impact problems [1–10, 70–73].

Acknowledgements This research was supported by the National Science Foundation (Projects # 1852510).

Data Availability Statement The data of the models developed in the paper are presented in the numerical example section.

Declarations

Conflict of interest The author declares that they have no conflict of interest.

References

1. Hartog, D.: Mechanical Vibration. McGraw-Hill, New York (1968)
2. Timoshenko, S.P., Goodier, J.N.: Theory of Elasticity. McGraw-Hill Book Co., Inc., New York (1970)
3. Dym, C.L., Shames, I.H.: Solid Mechanics: A Variational Approach. McGraw-Hill, New York (1973)
4. Timoshenko, S., Young, D.H., Weaver, W.: Vibration Problems in Engineering. Wiley, New York (1974)
5. Cook, R.D.: Concepts and Applications of Finite Element Analysis. Wiley, New York (1981)
6. Logan, D.L.: A First Course in the Finite Element Method, Chapter 15, 6th edn. Cengage Learning, Boston (2017)
7. Zienkiewicz, O.C.: The Finite Element Method. McGraw-Hill Company, London (1977)
8. Zienkiewicz, O.C., Taylor, R.L.: The Finite Element Method, Vol. 2: Solid Mechanics, vol.5., Butterworth-Heinemann, Oxford (2000).

9. Hallquist, J.O.: LS-DYNA Theory Manual. Livemore Software Technology Corporation, Livermore (2006)
10. Belytschko, T., Bindeman, L.P.: Assumed strain stabilization of the eight node hexahedral element. Comput. Methods Appl. Mech. Eng. **105**, 225–260 (1993)
11. Hussein, B.A., Sugiyama, H., Shabana, A.A.: Coupled deformation modes in the large deformation finite-element analysis: problem definition. ASME J. Comput. Nonlinear Dyn. **2**(2), 146–154 (2006)
12. Patel, M., Shabana, A.A.: Locking alleviation in the large displacement analysis of beam elements: the strain split method. Acta Mech. **229**(7), 2923–2946 (2018)
13. Sopanen, J.T., Mikkola, A.M.: description of elastic forces in absolute nodal coordinate formulation. Nonlinear Dyn. **34**(1–2), 53–74 (2003)
14. Johnson, W.: Helicopter Theory. Princeton University Press, New Jersey (1980)
15. Schilhans, M.J.: Bending frequency of a rotating cantilever beam. ASME, J. Appl. Mech. **25**, 28–30 (1958)
16. Kane, T.R., Ryan, R.R., Banerjee, A.K.: Dynamics of a cantilever beam attached to a moving base. AIAA J. Guid. Control Dyn. **10**(2), 139–151 (1987)
17. Wallrapp, O., Schwertassek, R.: Representation of geometric stiffening in multibody system simulation. Int. J. Numer. Methods Eng. **32**, 1833–1850 (1991)
18. Mayo, J., Dominguez, J.: Geometrically non-linear formulation of flexible multibody systems in terms of beam elements: geometric stiffness. Comput. Struct. **59**, 1039–1050 (1996)
19. Bakr, E.M., Shabana, A.A.: Geometrically nonlinear analysis of multibody systems. Comput. Struct. **23**, 739–751 (1986)
20. Garcia-Vallejo, D., Sugiyama, H., Shabana, A.A.: Finite element analysis of the geometric stiffening effect. parts 1 & 2. IMechE J. Multi-body Dyn. **219**, 187–211 (2005)
21. Sugawara, Y, Shinohara, K, Takagi, Y, Kobayas, N.: Experimental validation of numerical analysis on ANCF about dynamic stiffening effect of a two-dimensional beam. In: 5th Asian Conference on Multibody Dynamics 2010, Kyoto, Japan (2010)
22. Lugrís, U., Naya, M.A., Pérez, J.A., Cuadrado, J.: Implementation and efficiency of two geometric stiffening approaches. Multibody Syst. Dyn. **20**, 147–161 (2008). https://doi.org/10.1007/s11044-008-9114-6
23. Mayo, J.M., García-Vallejo, D., Domínguez, J.: Study of the geometric stiffening effect: comparison of different formulations. Multibody Syst. Dyn. **11**, 321–341 (2004). https://doi.org/10.1023/B:MUBO.0000040799.63053.d9
24. Cuadrado, J., Lugrís, U.: Implementation and efficiency of several geometric stiffening approaches. In: 12th IFToMM World Congress, Besançon (France), June 18–21, (2007)
25. Obrezkov, L.P., Matikainen, M.K., Harish, A.B.: A finite element for soft tissue deformation based on the absolute nodal coordinate formulation. Acta Mech. **231**, 1519–1538 (2020). https://doi.org/10.1007/s00707-019-02607-4
26. Ma, L., Wei, C., Zhao, Y.: Modeling and verification of a RANCF fluid element based on cubic rational bezier volume. ASME J. Comput. Nonlinear Dyn. **15**(4), 041005 (2020)
27. Piegl, L., Tiller, W.: The NURBS Book, 2nd edn. Springer, New York (1997)
28. ANSYS, 2015, Ansys Mechanical APDL Element Reference, Canonsburg, PA.
29. Kohnke, P.: Theory Reference for the Mechanical APDL and Mechanical Applications. PA, USA, ANSYS Inc, Canonsburg (2009)
30. Belytschko, T., Schwer, L., Klein, M.J.: Large displacement, transient analysis of space frames. Int. J. Numer. Methods Eng. **11**, 65–84 (1977)
31. Tian, Q., Zhang, Y.Q., Chen, L.P., Qin, G.: Advances in the absolute nodal coordinate method for the flexible multibody dynamics. Adv. Mech. **40**(2), 189–193 (2010)
32. Chen, Y., Zhang, D.G., Li, L.: Dynamic analysis of rotating curved beams by using absolute nodal coordinate formulation based on radial point interpolation method. J. Sound Vib. **441**, 63–83 (2019)
33. Nachbagauer, K.: State of the Art of ANCF elements regarding geometric description, interpolation strategies, definition of elastic forces, validation and locking phenomenon in comparison with proposed beam finite elements. Arch. Comput. Methods Eng. **21**(3), 293–319 (2014)
34. Shen, Z., Tian, Q., Liu, X., Hu, G.: Thermally induced vibrations of flexible beams using absolute nodal coordinate formulation. Aerospace Sci. Technol. **29**(1), 386–393 (2013)
35. Yu, L., Zhao, Z., Tang, J., Ren, G.: Integration of absolute nodal elements into multibody system. Nonlinear Dyn. **62**, 931–943 (2010)
36. Yu, H.D., Zhao, C.Z., Zheng, B., Wang, H.: A new higher-order locking-free beam element based on the absolute nodal coordinate formulation. J. Mech. Eng. Sci. **232**(9), 3410–3423 (2017)
37. Laflin, J.J., Anderson, K.S., Khan, I.M., Poursina, M.: New and extended applications of the divide-and-conquer algorithm for multibody dynamics. ASME J. Comput. Nonlinear Dyn. **9**(4), 1–8 (2014)
38. Tian, Q., Chen, L.P., Zhang, Y.Q., Yang, J.Z.: An efficient hybrid method for multibody dynamics simulation based on absolute nodal coordinate formulation. ASME J. Comput. Nonlinear Dyn. **4**(2), 021009-1-021009–14 (2009)
39. Yoo, W.S., Lee, J.H., Park, S.J., Sohn, J.H., Pogolev, D., Dmitrochenko, O.: Large deflection analysis of a thin plate: computer simulation and experiment. Multibody Syst. Dyn. **11**, 185–208 (2004)
40. Takahashi, Y., Shimizu, N., Suzuki, K.: Study on the frame structure modeling of the beam element formulated by absolute coordinate approach. J. Mech. Sci. Technol. **19**, 283–291 (2005)
41. Skrinjar, L., Slavic, J., Boltežar, M.: Absolute nodal coordinate formulation in a pre-stressed large-displacements dynamical system. J. Mech. Eng. **63**, 417–425 (2017). https://doi.org/10.5545/sv-jme.2017.4561
42. Ma, C., Wei, C., Sun, J., Liu, B.: Modeling method and application of rational finite element based on absolute nodal coordinate formulation. Acta Mech. Solida Sinica (2018). https://doi.org/10.1007/s10338-018-0020-z
43. Fotland, G., Haskins, C., Rølvåg, T.: Trade study to select best alternative for cable and pulley simulation for cranes on offshore vessels. Syst. Eng. **23**, 177–188 (2019). https://doi.org/10.1002/sys.21503
44. Li, S., Wang, Y., Ma, X., and Wang, S.: Modeling and simulation of a moving yarn segment: based on the absolute

nodal coordinate formulation. Mathematical Problems in Engineering, Vol. 2019, Article ID 6567802 (2019). https://doi.org/10.1155/2019/6567802.
45. Pan, K., Cao, D.: Absolute nodal coordinate finite element approach to the two-dimensional liquid sloshing problems. Proc. Inst. Mech. Eng. Part K J. Multi-body Dyn. **234**(2), 1–25 (2020). https://doi.org/10.1177/1464419320907785
46. Yamano, A.A., Shintani, A., Ito, T., Nakagawa, C., Ijima, H.: Influence of boundary conditions on a flutter-mill. J. Sound Vib. **478**, 115359 (2020)
47. Hewlett, J.: Methods for real-time simulation of systems of rigid and flexible bodies with unilateral contact and friction", Ph.D. Thesis, Department of Mechanical Engineering, McGill University (2019).
48. Hewlett, J., Arbatani, S., Kovecses, J.: A fast and stable first-order method for simulation of flexible beams and cables. Nonlinear Dyn. **99**, 1211–1226 (2020)
49. Shen, Z.X., Li, P., Liu, C., Hu, G.K.: A finite element beam model including cross-section distortion in the absolute nodal coordinate formulation. Nonlinear Dyn. **77**(3), 1019–1033 (2014)
50. Shen, Z., Liu, C., Li, H.: Viscoelastic analysis of bistable composite shells via absolute nodal coordinate formulation. Compos. Struct. (2020). https://doi.org/10.1016/j.compstruct.2020.112537
51. Htun, T.Z., Suzuki, H., Garcia-Vallejo, D.: Dynamic modeling of a radially multilayered tether cable for a remotely-operated underwater vehicle (ROV) based on the absolute nodal coordinate formulation (ANCF). Mech. Mach. Theory **153**, 103961 (2020). https://doi.org/10.1016/j.mechmachtheory.2020.103961
52. Zhang, W., Zhu, W., Zhang, S.: Deployment dynamics for a flexible solar array composed of composite-laminated plates. ASCE J. Aerosp. Eng. **33**, 1–21 (2020)
53. Sheng, F., Zhong, Z., Wang, K.: Theory and model implementation for analyzing line structures subject to dynamic motions of large deformation and elongation using the absolute nodal coordinate formulation (ANCF) approach. Nonlinear Dyn. (2020). https://doi.org/10.1007/s11071-020-05783-4
54. Wang, J., Wang, T.: Buckling analysis of beam structure with absolute nodal coordinate formulation. IMechE J. Mech. Eng. Sci. (2020). https://doi.org/10.1177/0954406220947117
55. Yuan, T., Liu, Z., Zhou, Y., Liu, J.: Dynamic modeling for foldable origami space membrane structure with contact-impact during deployment. Multibody Syst. Dyn. **50**, 1–24 (2020)
56. Zhao, C.H., Bao, K.W., Tao, Y.L.: Transversally higher-order interpolating polynomials for the two-dimensional shear deformable ANCF beam elements based on common coefficients. Multibody Syst. Dyn. (2020). https://doi.org/10.1007/s11044-020-09768-4
57. Omar, M.A., Shabana, A.A.: A two-dimensional shear deformable beam for large rotation and deformation problems. J. Sound Vib. **243**(3), 565–576 (2001)
58. Shabana, A.A.: Computational Continuum Mechanics, 3rd edn. Wiley, Chichester, UK (2018)
59. Shabana, A.A., Eldeeb, A.E.: Motion and shape control of soft robots and materials. Nonlinear Dyn (2021). https://doi.org/10.1007/s11071-021-06272-y
60. Babuska, I., Suri, M.: On locking and robustness in the finite element method. SIAM J Numer Anal **29**(5), 1261–1293 (1992)
61. Carpenter, N., Belytschko, T., Stolarski, H.: Locking and shear scaling factors in bending elements. Comput Struct **22**(1), 39–52 (1986)
62. Rakowski, J.: The interpretation of the shear locking in beam elements. Comput Struct **37**(5), 769–776 (1990)
63. Raveendranath, P., Singh, G., Pradhan, B.: A two-noded locking-free shear flexible curved beam element. Int J Numer Methods Eng **44**(2), 265–280 (1999)
64. Stolarski, H., Belytschko, T.: Shear and membrane locking in curved elements. Comput Methods Appl Mech Eng **41**(3), 279–296 (1983)
65. Shabana, A.A., Desai, C.J., Grossi, E., Patel, M.: Generalization of the strain-split method and evaluation of the nonlinear ancf finite elements. Acta Mech **231**, 1365–1376 (2020)
66. Trivedi, D., Dienno, D., Rahn, C.D.: Optimal, model-based design of soft robotic manipulators. ASME J. Mech. Des. **130**, 091402-1-091402–9 (2008)
67. Shabana, A.A., Zhang, D.: ANCF multiplicative-decomposition thermoelastic approach for arbitrary geometry. ASCE J. Struct. Eng. (2021)
68. Maqueda, L.G., Shabana, A.A.: Poisson modes and general nonlinear constitutive models in the large displacement analysis of beams. J. Multibody Syst. Dyn. **18**(3), 375–396 (2007)
69. Petrolo, A.S., Casciaro, R.: 3D beam element based on saint Venànt's Rod theory. Comput. Struct. **82**, 2471–2481 (2004). https://doi.org/10.1016/j.compstruc.2004.07.004
70. Meirovitch, L.: Elements of Vibration Analysis. McGraw-Hill, New York (1986)
71. Shabana, A.A.: Vibration of Discrete and Continuous Systems, 3rd edn. Springer, New York (2019)
72. Thomson, W.T.: Theory of Vibration with Applications. Prentice Hall, Englewood Cliffs, NJ (1988)
73. Khulief, Y.A., Shabana, A.A.: Impact responses of multi-body systems with consistent and lumped masses. Sound Vib. **104**, 187–207 (1986)